Available online at www.sciencedirect.com
SCIENCE DIRECT®
Journal of Magnetic Resonance 172 (2005) 63–78
JMR Journal of Magnetic Resonance
www.elsevier.com/locate/jmr

Practical pulse synthesis via the discrete inverse scattering transform☆

Jeremy Magland, Charles L. Epstein*

Department of Mathematics and LSNI, University of Pennsylvania, Philadelphia, PA, United States

Received 8 January 2004; revised 3 September 2004

Abstract

This paper provides the practical details required to use the inverse scattering (IST) approach to design selective RF-pulses. As in the Shinnar–Le Roux (SLR) approach, we use a hard pulse approximation to actually design the pulse. Unlike SLR, the pulse is designed using the full inverse scattering data (the reflection coefficient and the bound states) rather than the flip angle profile. We explain how to approximate the reflection coefficient to obtain a pulse with a prescribed rephasing time. In contrast to the SLR approach, we retain direct control on the phase of the magnetization profile throughout the design process. We give explicit recursive algorithms for computing the hard pulse from the inverse scattering data. These algorithms are quite different from the SLR recursion, being essentially discretizations of the Marchenko equations. We call our approach the discrete inverse scattering transform or DIST. Overall, it is as fast as the SLR approach. When bound states are present, we use both the left and right Marchenko equations to improve the numerical stability of the algorithm. We compute a variety of examples and consider the effect of amplitude errors on the magnetization profile.

Keywords: Nuclear magnetic resonance; Inverse scattering; RF-pulse design; Hard pulse approximation; Discrete inverse scattering transform; Discrete Marchenko equation; Bound states; Reflection coefficient

1. Introduction

The design of a selective RF-pulse starts with a magnetization profile $\boldsymbol{M}(v)$, which is a unit 3-vector valued function of the offset frequency v. The goal is to find an RF-pulse $\boldsymbol{B}_1(t)$ that, after rephasing, produces the specified magnetization profile. If the background field points along the laboratory z-direction, then the RF-pulse is of the form

$$B_1(t) = [e^{i\omega_0 t}(\omega_1(t) + i\omega_2(t)), 0]. \quad (1)$$

Here, and in the sequel, we follow the common practice in MR of representing the transverse components, i.e., x and y components, of a 3-vector as a complex number.

In [2], Buonocore showed that essentially all known methods of direct pulse design could be interpreted as implementations of the inverse scattering transform for the spin domain Bloch equation. The algorithms differ in how they use the input data, $\boldsymbol{M}(v)$, to obtain scattering data for the Bloch equation and in the numerical techniques used to solve the inverse scattering problem. We refer the reader to [2] for detailed descriptions of these approaches. The inverse scattering approach to pulse design is described in [1–4,11].

This paper presents a new algorithm for implementing the inverse scattering transform as a method for selective RF-pulse design. As with the layer stripping method and the Shinnar–Le Roux algorithm, we employ a hard pulse approximation. Our approach is, in a real sense, a synthesis of the SLR method, as described for

☆ Research of both authors partially supported by NSF Grant DMS02–07123, C.L.E. partially supported by the Francis J. Carey term chair.
* Corresponding author.
E-mail addresses: jfm@math.upenn.edu (J. Magland), cle@math.upenn.edu (C.L. Epstein).

1090-7807/$ - see front matter © 2004 Elsevier Inc. All rights reserved.
doi:10.1016/j.jmr.2004.09.022

example in [7,13,14], and the inverse scattering approach. After a rapid review of the concepts used in inverse scattering, we give a more detailed comparison of our algorithm with the earlier approaches. For the most part we assume that the reader is familiar with [4].

Basic to essentially all direct approaches to pulse design is the spin domain Bloch equation for a pair of complex valued functions $\boldsymbol{\psi}(\xi;t) = (\psi_1(\xi;t), \psi_2(\xi;t))$

$$\frac{\mathrm{d}\boldsymbol{\psi}}{\mathrm{d}t}(\xi;t) = \begin{bmatrix} -\mathrm{i}\xi & q(t) \\ -q^*(t) & \mathrm{i}\xi \end{bmatrix} \boldsymbol{\psi}(\xi;t). \tag{2}$$

If v denotes the offset frequency in the rotating reference frame, then

$$\xi = \frac{v}{2}, \quad q(t) = \frac{-\mathrm{i}\gamma}{2}(\omega_1(t) - \mathrm{i}\omega_2(t)), \tag{3}$$

where ω_1, ω_2 come from Eq. (1). The $\mathbb{C}^2$-valued function $\boldsymbol{\psi}(\frac{1}{2}v;t)$ is the spin domain representation of the magnetization state, at time t, of the spins with offset frequency v. It is usually assumed that $q(t)$ is an absolutely integrable function, in which case, the solution $\boldsymbol{\psi}(\xi;t)$ is a continuous function of t.

1.1. Scattering for the spin-domain Bloch equation

Let $\boldsymbol{\psi}_-(\xi;t)$ denote the solution of Eq. (2) asymptotic to $[\mathrm{e}^{-\mathrm{i}\xi t}, 0]$, as t goes to $-\infty$. As $t \to +\infty$, this solution is asymptotic to a vector valued function of the form

$$[a(\xi)\mathrm{e}^{-\mathrm{i}\xi t}, b(\xi)\mathrm{e}^{\mathrm{i}\xi t}]. \tag{4}$$

The functions $(a(\xi), b(\xi))$ are the *scattering coefficients* defined by q. The *reflection coefficient* is defined to be

$$r(\xi) = \frac{b(\xi)}{a(\xi)}. \tag{5}$$

As noted above, the input to an RF-pulse design problem is $\boldsymbol{M}(\xi)$, a unit 3-vector valued function defined on $\mathbb{R}$. In the spin-domain formalism, the goal of RF-pulse design is to find $q(t)$ so that the reflection coefficient satisfies

$$r(\xi) = \frac{\boldsymbol{M}_x(\xi) + \mathrm{i}\boldsymbol{M}_y(\xi)}{1 + \boldsymbol{M}_z(\xi)}. \tag{6}$$

In the sequel, the expression "phase of the magnetization profile" refers to the phase of $\boldsymbol{M}_x(\xi) + \mathrm{i}\boldsymbol{M}_y(\xi)$, which equals the phase of $r(\xi)$.

There are, in fact, infinitely many functions $q(t)$ that produce a given magnetization profile. The inverse scattering formalism gives a description of the space of such functions as well as an algorithm, in principle, for finding them. In addition to $r(\xi)$, for $\xi \in \mathbb{R}$, a solution to the inverse scattering problem is specified by a finite collection of pairs of complex numbers $\{(\xi_1, C_1), \ldots, (\xi_m, C_m)\}$. Each pair (ξ_j, C_j) defines a *bound state*. The number m can be any natural number or zero, each ξ_j has positive imaginary part, and each C_j is nonzero. The data $\{r(\xi);(\xi_1, C_1), \ldots, (\xi_m, C_m)\}$ is called the reduced scattering data. The map that goes from this data to the unique potential it defines is called the inverse scattering transform (IST). It is described in detail in [4].

1.2. Inverse scattering for the spin-domain Bloch equation

In MR applications one usually assumes that $r(\xi)$ is a reasonably smooth function with bounded support. The IST then produces a reasonably smooth potential with fairly rapid decay. There are many ways to practically implement the IST. Among them, the Marchenko equation formalism, which is described in Sections 5 and 6 of [4]. Briefly, for each $t \in \mathbb{R}$, one defines an integral operator, F_t, acting on $L^2([t,\infty))$. One must then solve an integral equation, called the Marchenko equation, of the form

$$(\mathrm{Id} + F_t^* F_t)k_t(s) = f^*(t+s). \tag{7}$$

The function $q(t)$ is then found by setting $q(t) = -2k_t(t)$. In our earlier paper we described an iterative approach to solving these equations. While, in principle, this approach should work for any reasonable data, in practice it is unstable and slow. This is not simply a fault of our implementation, but rather a reflection of the fact that, in this context, the IST itself is rather ill conditioned. In this paper, we give the details of an algorithm for approximately implementing the inverse scattering transform that is both stable and efficient.

1.3. The hard pulse approximation

As in the SLR and layer stripping approaches, we use a hard pulse approximation. This means that we design an RF-envelope that is a series of hard pulses:

$$q_\Omega(t) = \sum_{j=-\infty}^{\infty} \mu_j \delta(t - j\Delta). \tag{8}$$

Here and in the sequel, the subscript Ω refers to the sequence of coefficients, $\{\mu_j\}$. As we explain in the next two sections, there is a reasonable discrete analogue of the Bloch equation and both its forward and inverse scattering theories for potentials of this singular, but special, form. The scattering coefficients, a and b are periodic functions of period $\Delta^{-1}\pi$, and therefore can be expressed as functions of $w = \mathrm{e}^{2\mathrm{i}\xi\Delta}$. The bound states are determined by the zeros of $a(w)$ inside the unit disk. We use this discrete inverse scattering theory to derive our algorithm.

An advantage of using hard pulses is that, for this kind of data, the IST can be realized by an exact algebraic recursion. One thereby diminishes the instabilities inherent in the usual iterative numerical approaches to the Marchenko equation. In practical applications, a "softened" version of $q_\Omega(t)$ is actually implemented. In order for the softened pulse to produce a magnetization profile close to that produced by $q_\Omega(t)$, it is necessary

that the coefficients $\{\mu_j\}$ be uniformly small. As these coefficients are $O(\Delta)$, this reduces to the requirement that the time step, Δ, be sufficiently small. This is what is often called the *hard pulse approximation*. Given $\boldsymbol{M}(\xi)$, a time step Δ is selected so that $\boldsymbol{M}(\xi) = [0, 0, 1]$ outside the interval $[-\frac{\pi}{2\Delta}, \frac{\pi}{2\Delta}]$. To use the hard pulse approximation, $\boldsymbol{M}$ is replaced with the 2π-periodic function defined by

$$\boldsymbol{M}^p(w) = \boldsymbol{M}\left(\frac{\log w}{2i\Delta}\right) \quad \text{with} \quad -i\log w \in [-\pi, \pi]. \tag{9}$$

It is at this point that the different approaches start to diverge. In the SLR approach the next step is to find a polynomial $B(w)$, so that $|B(w)|$ approximates

$$|B(w)| = \sqrt{\frac{1 - \boldsymbol{M}_z^p(w)}{2}}. \tag{10}$$

Note that the flip angle profile is given by $\varphi(\xi) = 2\sin^{-1}(|b(\xi)|)$. Finding $B(w)$ is a "polynomial design" problem. The particular technique used to solve it determines, implicitly, the phase of $B(w)$. A second polynomial $A(w)$ of the same degree is then determined so that $|A(w)|^2 + |B(w)|^2 = 1$. In the layer stripping method, one generally finds a polynomial $R(w)$ that approximates the reflection coefficient $r(\xi)$ defined in (6). In our approach we also find an approximation to $r(\xi)$, though it is not restricted to be a polynomial in w, and one is also free to specify the data connected to bound states. To a limited extent, bound states can also be incorporated in the layer stripping method, though, to the best of our knowledge, this possibility has not been explored in the literature.

In all cases, the final step is to use a recursion to determine the coefficients $\{\mu_j\}$ from the scattering data. Our recursion differs from both the SLR transform and the layer stripping method as is explained in Section (4). In SLR, if A and B are of degree N, then the pulse is of duration $N\Delta$. Ideally one would like to have

$$\frac{B(w)}{A(w)} \approx r\left(\frac{\log w}{i2\Delta}\right). \tag{11}$$

As explained in [4], by designing $|B(w)|$ as an approximation to $\sqrt{(1 - \boldsymbol{M}_z^p(w))/2}$, with the design technique determining the phase of $B(w)$, one sacrifices direct control over the phase of $R(w)$, and hence over the phase of transverse magnetization profile. For simple pulses this phase error is often approximately linear over the pass band and can be diminished by adjusting the rephasing time.

A principal difference between our approach and the SLR approach is that we work directly with the reflection coefficient. To design a minimum energy pulse we might use a Remez-type algorithm to approximate r itself by a polynomial function of w. (The Remez approach to polynomial approximation is described in [10] and its application to filtering theory in [9].) To some extent, we sacrifice direct control on the duration of the pulse. To be more precise: while the full duration of the pulse is not specified in advance, we do control the rephasing time of the designed pulse. In practice, a 90° slice selective pulse designed using the IST approach has a slightly longer duration than an SLR pulse with comparable design parameters. Generally, the IST pulse produces a markedly cleaner, and more accurate magnetization profile.

In the pulse design problem, only the reflection coefficient is specified. In the inverse scattering problem, one is also free to specify bound states. The bound states arise only implicitly in the SLR formalism [8]. Moreover, in the SLR approach, the introduction of bound states leads to further errors in the phase of the transverse magnetization. In our approach the bound states are auxiliary data, which do not change the magnetization profile. Our algorithm therefore captures the true nonuniqueness of the solution to the pulse design problem as explained in [4]. Once a magnetization profile is fixed, the flexibility in designing different pulses to attain the target profile lies mostly in the selection of bound states. While it remains unclear how this should be done, our algorithm makes it possible to explore the possibilities in a systematic way.

The recursion we use to determine the coefficients $\{\mu_j\}$ from $r(w)$ and the bound state data is philosophically quite different from the SLR recursion. It is inspired by the Marchenko equation formalism. The introduction of bound states often leads to ill conditioned problems, with exponentially growing condition number. An important aspect of our approach is that we use both the left and right Marchenko equations, see Section 6 of [4]. While ill conditioned systems still arise, they remain amenable to recursive numerical solution.

The paper is organized as follows: the next section introduces concepts and notation connected to the analysis of hard pulses. In the following section we state discrete versions of the left and right Marchenko equations. In the continuum case, these equations are usually stated in the time domain, e.g., see Eqs. (59) and (68) in [4]. In this paper, we state the discrete Marchenko equations in the Fourier domain. We use the Fourier domain formulation because it is simpler and leads more rapidly to algorithms for obtaining pulses. An exposition of the Fourier domain approach for the continuum problem can be found in Chapter II of [5] or [6]. We next give recursive algorithms to go from reduced scattering data to the pulse. After deriving the algorithm, we give a variety of examples. Several mathematical results are proved in the Appendix.

Conventions used in the figures. The pulse plots are all in the rotating frame, that is, if, in the laboratory frame $B_1(t) = (\omega_1(t) + i\omega_2(t))e^{i\omega_0 t}$, then our plots show $\omega_1(t)$ and $\omega_2(t)$. In most cases only $\omega_1(t)$ is nonzero. The real part $\omega_1(t)$ is shown as a solid line, while the imaginary

part $\omega_2(t)$, is shown as a dot-dash line. In the plots of transverse magnetization profiles the x-component is shown with a solid line and the y-component with a dot-dash line. In several plots we show the full magnetization profile; in these plots the z-component is shown with a dashed line.

2. Scattering theory for hard pulses

For a series of hard pulses, a solution to Eq. (2) is no longer continuous but instead has jump discontinuities. These occur at the times, $j\Delta$, for which $\mu_j \neq 0$. The evolution of $\boldsymbol{\psi}(\xi;t)$, for t in the intervals $(j\Delta,(j+1)\Delta)$, is simply free precession. With that in mind, we replace the continuum Bloch equation with a discrete analogue. A bi-infinite sequence of pairs of complex valued functions $(A_j(w),B_j(w))$ solves the discrete Bloch equation with potential $q_\Omega(t)$, given in Eq. (8), if, for each $j \in \mathbb{Z}$ and w on the unit circle, we have

$$\begin{bmatrix} A_{j+1}(w) \\ B_{j+1}(w) \end{bmatrix} = \begin{bmatrix} \alpha_j & -\beta_j^* \\ w\beta_j & w\alpha_j \end{bmatrix} \begin{bmatrix} A_j(w) \\ B_j(w) \end{bmatrix}. \tag{12}$$

This equation is equivalent to Eq. (18) in [2]. Here

$$\begin{aligned} \beta_j &= \frac{\mu_j^*}{|\mu_j|}\sqrt{\frac{1-\cos|\mu_j|}{2}}, \\ \alpha_j &= \sqrt{1-|\beta_j|^2} = \sqrt{\frac{1+\cos|\mu_j|}{2}}. \end{aligned} \tag{13}$$

Up to a normalization, this is nothing but the relation describing the jumps, at integer multiples of Δ, in the distributional solution of the Bloch equation with the potential $q_\Omega(t)$.

As with the continuum case, the scattering and inverse scattering theories for this recursion equation rely on the possibility of finding solutions to Eq. (13), normalized as j goes to $\pm\infty$, with analyticity properties in w. Under mild hypotheses on the coefficients $\{\mu_j\}$, there are unique solutions $[A_{\pm,j}(w), B_{\pm,j}(w)]$ to Eq. (13) such that

$$\lim_{j\to\infty} \begin{bmatrix} A_{+,j}(w) \\ B_{+,j}(w) \end{bmatrix} = \begin{bmatrix} 1 \\ 0 \end{bmatrix}, \quad \lim_{j\to-\infty} \begin{bmatrix} A_{-,j}(w) \\ B_{-,j}(w) \end{bmatrix} = \begin{bmatrix} 1 \\ 0 \end{bmatrix}. \tag{14}$$

The functions $\{A_{-,j}(w), w^{-1}B_{-,j}(w), A_{+,j}^*(w), B_{+,j}^*(w)\}$ have analytic extensions to the unit disk. These analyticity properties mirror those of the normalized solutions to the continuum Bloch equation and are essential for the success of the inverse approach.

The analogue of the scattering operator is easiest to express in terms of the 2×2 matrices

$$V_{\pm,j} = \begin{bmatrix} A_{\pm,j}(w) & -B_{\pm,j}^*(w) \\ B_{\pm,j}(w) & A_{\pm,j}^*(w) \end{bmatrix} \begin{bmatrix} w^{-j/2} & 0 \\ 0 & w^{j/2} \end{bmatrix}. \tag{15}$$

In [6] it is shown that there are functions $a(w)$, $b(w)$ so that

$$|a(w)|^2 + |b(w)|^2 = 1 \tag{16}$$

and, for any $j \in \mathbb{Z}$, and w on the unit circle we have the relation

$$s_\Omega(w) = \begin{bmatrix} a(w) & -b^*(w) \\ b(w) & a^*(w) \end{bmatrix} = V_{+,j}^* V_{-,j}. \tag{17}$$

The matrix $s_\Omega(w)$ is the discrete analogue of the scattering matrix. As in the continuum case, the function $a(w)$ has an analytic extension to the unit disk and finitely many zeros. Moreover $a(0)$ is a positive real number. We define the reflection coefficient as the ratio

$$r(w) = \frac{b(w)}{a(w)}. \tag{18}$$

If $\{\zeta_1,\ldots,\zeta_m\}$ are the zeros of a in the unit disk, then, as in the continuum case, using Eq. (16), a can be determined from r

$$a(w) = \prod_{k=1}^{m} \left(\frac{|\zeta_k|}{\zeta_k}\frac{\zeta_k - w}{1-\zeta_k^* w}\right) \exp\left(-\tilde{\Pi}_+[\log(1+|r(w)|^2)]\right), \tag{19}$$

see Eq. (4) in [4]. The action of the operator $\tilde{\Pi}_+$ is easily expressed in terms of Fourier series as follows:

$$\tilde{\Pi}_+\left(\sum_{n=-\infty}^{\infty} f_n w^n\right) = \frac{1}{2}f_0 + \sum_{n=1}^{\infty} f_n w^n. \tag{20}$$

If $f(w)$ is a function on the unit circle, then $\tilde{\Pi}_+ f(w)$ is the part of f with an analytic extension to the unit disk.

The potential $q_\Omega(t)$ is not quite determined by the reflection coefficient $r(w)$ and the locations of the zeros of $a(w)$ inside the unit disk. As in the continuum case, one also needs to specify m nonzero complex numbers, $\{c_1,\ldots,c_m\}$, which we call the *discrete norming constants*. The collection of data

$$r(w) \quad \text{for } |w| = 1 \text{ and } \{(\zeta_1,c_1),\ldots,(\zeta_m,c_m)\} \tag{21}$$

is called the *reduced scattering data*. In the next section we show how to reconstruct a hard pulse from such a collection of data.

If the pulse $q_\Omega(t)$ is finite sum with N terms, then it is easy to compute that

$$a = \sum_{n=0}^{N-1} a_j w^j \quad \text{and} \quad b = \sum_{j=1-\rho}^{N-\rho} b_j w^j. \tag{22}$$

The significance of the number ρ is that this pulse requires ρ rephasing time steps, of length Δ, to achieve the magnetization profile specified by $r(w) = b(w)/a(w)$. This is the sort of data that arise in SLR pulse design. More generally a hard pulse of the form

$$q_\Omega(t) = \sum_{j=-\infty}^{\rho-1} \mu_j \delta(t - j\Delta), \tag{23}$$

requires ρ rephasing time steps and has scattering data of the form

$$a = \sum_{n=0}^{\infty} a_j w^j \quad \text{and} \quad b = \sum_{j=1-\rho}^{\infty} b_j w^j. \tag{24}$$

Data of the type given in Eq. (24) naturally arise in IST pulse design. As $j \to -\infty$ the coefficients $\{\mu_j\}$ typically tend to zero very rapidly. Hence, the pulse can be truncated to have finite length without significantly altering the magnetization profile. We return to this question in Section (4.3). For a general bi-infinite hard pulse, the scattering coefficients are of the form

$$a = \sum_{n=0}^{\infty} a_j w^j \quad \text{and} \quad b = \sum_{j=-\infty}^{\infty} b_j w^j. \tag{25}$$

Data of this sort arise when one seeks to specify the bound state data in a manner unconnected to the reflection coefficient. In all cases the coefficients $a(w)$, $b(w)$ satisfy Eq. (16).

To complete our discussion of scattering theory, we state the analogue of the energy formula for a continuum pulse given in [4,12]:

$$\sum_{j=-\infty}^{\infty} \log(1+|\gamma_j|^2) = \frac{1}{2\pi}\int_0^{2\pi} \log(1+|r(\mathrm{e}^{\mathrm{i}\theta})|^2)\,\mathrm{d}\theta - 2\sum_{k=1}^{m} \log|\zeta_k|, \tag{26}$$

Here $\{\zeta_1,\ldots,\zeta_m\}$ are the zeros of $a(w)$ in the unit disk and

$$\gamma_j = \frac{\beta_j}{\alpha_j}, \tag{27}$$

see Eq. (13). Provided that $|\gamma_j| < 1$, μ_j can be recovered from γ_j by using the formula

$$\mu_j = \frac{\gamma_j^*}{|\gamma_j|}\arcsin\frac{2|\gamma_j|}{1+|\gamma_j|^2}. \tag{28}$$

In the absence of bound states, a related, though somewhat less explicit formula appears in [7]. This formula and the facts from scattering theory enumerated above are proved in [6].

3. Inverse scattering theory for hard pulses

In this section, we state an analogue of the Marchenko equations for obtaining a hard pulse with given reduced scattering data. We call our new method, the discrete inverse scattering transform or DIST. In this section we assume that the reduced scattering data is given. A reader unconcerned with the mathematical details leading up to the DIST recursion may safely skip to Section 4.

3.1. The discrete inverse scattering approach

In the discrete inverse scattering approach, the input data is a reflection coefficient $r(w)$, which is defined as a Fourier series on the unit circle, along with data specifying the bound states, $\{(\zeta_1,c_1),\ldots,(\zeta_m,c_m)\}$. In this paper, we assume that the $\{\zeta_k\}$ are distinct points in the unit disk. The general case is treated in [6]. In the remainder of this section we present analogues of the Marchenko equations *in the Fourier domain*. In the continuum case, this is Eq. (5) in [2].

The method we give for obtaining Ω from $s_\Omega(w)$ works with arbitrary scattering data; it does not require $a(w)$ and $b(w)$ to be polynomials. Given the reflection coefficient, as a Fourier series, this method is also recursive, though the actual recursion is quite different from that used in SLR. Our algorithm makes extensive usage of the projection operators, $\Pi_\pm$. We define these operators acting on functions defined on the unit circle $|w| = 1$. In terms of Fourier series they are given by:

$$\Pi_-\left(\sum_{n=-\infty}^{\infty} f_n w^n\right) = \sum_{n=-\infty}^{-1} f_n w^n \quad \text{and} \quad \Pi_+\left(\sum_{n=-\infty}^{\infty} f_n w^n\right) = \sum_{n=1}^{\infty} f_n w^n. \tag{29}$$

The projection Π_+ projects onto functions with an analytic extension to the unit disk vanishing at $w = 0$, whereas Π_- projects onto functions with an analytic extension to the exterior of the unit disk vanishing at $w = \infty$.

3.2. The right discrete Marchenko equation

We now state the right discrete Marchenko equations in the Fourier domain. To do so, we define a collection of functions $\{r_j(w) : j \in \mathbb{Z}\}$ using the reflection coefficient $r(w)$ and the pairs in (21): for $j \in \mathbb{Z}$ define

$$r_j(w) = \Pi_-(r(w)w^{j-1}) - \sum_{k=1}^{m} \frac{c_k\zeta_k^{j-1}}{w-\zeta_k}. \tag{30}$$

If there are no bound states then the finite sum in Eq. (30) is absent. The right discrete Marchenko equations are:

$$A_{+,j} = \hat{A}_{+,j}(0) + \Pi_-\left(r_j(w^{-1}B_{+,j})^*\right), \tag{31}$$

$$w^{-1}B_{+,j} = -\Pi_-\left(r_j A_{+,j}^*\right). \tag{32}$$

These equations can be combined into a single equation:

$$(1+\Pi_+ r_j^*\Pi_- r_j)\left(\frac{wB_{+,j}^*}{\hat{A}_{+,j}(0)}\right) = -\Pi_+ r_j^*. \tag{33}$$

A detailed derivation of these equations in given in [6].

It is not difficult to prove that Eq. (33) has a unique solution. Using the inverse of the recursion in Eq. (12), and the fact that the constant term of $B_{+,j}(w)$ must vanish we see that

$$\gamma_j = \frac{\hat{B}_{+,j}(1)}{\hat{A}_{+,j}(0)}. \tag{34}$$

Thus γ_j could be obtained from the first Fourier coefficient of the solution to the Marchenko equation (33). The pulse could then be computed using Eq. (28). One could therefore generate the pulse by solving the equations in (33) directly. We show in Section 3.4 that there is a recursive algorithm for determining γ_j. This algorithm is much more efficient and stable than directly solving Eq. (33).

3.3. The left discrete Marchenko equation

Eq. (33) is the discrete analogue of the right Marchenko equation. As in the continuum case, there is also a left Marchenko equation. When there are nontrivial bound states, it is important to use both equations to control the instability that arises from these ill conditioned linear systems. In this section we state the analogue of the left Marchenko equation, which gives a recursion for determining $\{\gamma_j\}$ in terms of $A_{-,j}$ and $B_{-,j}$.

The left Marchenko equation is

$$(1 + \Pi_+ s_j^* \Pi_- s_j)\left(\frac{B_{-,j}}{\hat{A}_{-,j}(0)}\right) = -\Pi_+ s_j^*, \tag{35}$$

where:

$$\begin{aligned} s(w) &= \frac{-b^*(w)}{a(w)}, \\ s_j(w) &= \Pi_-(sw^{-j}) - \sum_{k=1}^{m} \frac{\tilde{c}_k \zeta_k^{-j}}{w - \zeta_k}. \end{aligned} \tag{36}$$

Here the "left norming constants," $\{\tilde{c}_k\}$ are given by

$$\tilde{c}_k = -\frac{\zeta_k^{-1}}{c_k [a'(\zeta_k)]^2}. \tag{37}$$

The left equation becomes necessary in circumstances where the right equation becomes numerically unstable, e.g., when there are bound states. In order for the solution obtained using the left equation to match up with that obtained using the right equation, it is very important that $s(w)$ and $\{\tilde{c}_k\}$ are computed accurately. Note that the coefficients $\{\tilde{c}_k\}$ depend upon $\{a'(\zeta_k)\}$. The evaluation of these derivatives is often the most delicate and demanding step in utilizing the left equation. In general this is not possible if one does not know the exact locations of the roots. In Section 4.2, we give a representation for the right scattering data with an algorithm to accurately and efficiently determine the left scattering data.

3.4. A recursive algorithm for DIST

We now give a recursive algorithm for the determination of $\{\gamma_j\}$. Equation (12) can be rewritten:

$$\begin{bmatrix} A_{+,j} \\ B_{+,j} \end{bmatrix} = \alpha_j \begin{bmatrix} 1 & \gamma_j^* w^{-1} \\ -\gamma_j & w^{-1} \end{bmatrix} \begin{bmatrix} A_{+,j+1} \\ B_{+,j+1} \end{bmatrix}. \tag{38}$$

Plugging this formula into Eq. (32) and using the fact that, $\Pi_- r_j w = r_{j+1}$, we get

$$\begin{aligned} -\gamma_j A_{+,j+1} + w^{-1} B_{+,j+1} = &-w\Pi_- r_j A_{+,j+1}^* \\ &- \gamma_j w \Pi_- r_j (w^{-1} B_{+,j+1})^*. \end{aligned} \tag{39}$$

Examining the constant coefficient of both sides of this equation we find that

$$-\gamma_j \hat{A}_{+,j+1}(0) = -\mathcal{F}(r_j A_{+,j+1}^*)(-1) - \gamma_j \mathcal{F}(r_j w B_{+,j+1}^*)(-1) \tag{40}$$

$$= -\mathcal{F}(w r_j A_{+,j+1}^*)(0) - \gamma_j \mathcal{F}(w r_j w B_{+,j+1}^*)(0). \tag{41}$$

Here $\mathcal{F}(h)(n)$ denotes the coefficient of w^n in the Fourier series of h. Solving for γ_j gives:

$$\gamma_j = \frac{\mathcal{F}(w r_j A_{+,j+1}^*)(0)}{\hat{A}_{+,j+1}(0) - \mathcal{F}(w r_j (w^{-1} B_{+,j+1})^*)(0)}. \tag{42}$$

Thus we can reconstruct $A_{+,j}$ and $B_{+,j}$ from $A_{+,j+1}$ and $B_{+,j+1}$ by using this expression for γ_j along with the recursion 38. To begin the recursion, we assume that, at a sufficiently large value of $j = \rho$:

$$\begin{aligned} A_{+,\rho}(w) &\approx 1, \\ B_{+,\rho}(w) &\approx 0. \end{aligned} \tag{43}$$

The pulse is then obtained using Eq. (28). If the pulse requires ρ rephasing time steps then the $\approx$ in Eq. (43) is actually an equality.

One can now appreciate a fundamental difference between the SLR recursion, the layer stripping method and the DIST recursion. As explained on p. 474 in [2], the SLR transform and layer stripping method both begin using all the scattering data and the recursion peels it away. Using DIST we start with Eq. (43), so the initial data is trivial. Our recursion uses the scattering data to build up the solution. This shows that our method is indeed a different algorithm from those previously known.

Applying the method employed above with the left Marchenko equation, we obtain

$$-\gamma_{j-1}^* = \frac{\mathcal{F}(w s_j A_{-,j-1})(0)}{\hat{A}_{-,j-1}(0) - \mathcal{F}(w s_j B_{-,j-1})(0)}. \tag{44}$$

Starting with $A_{-,j-1}$ and $B_{-,j-1}$, one can reconstruct $\{\gamma_j\}$ and $A_{-,j}$ and $B_{-,j}$ from s and $\{(\zeta_k, \tilde{c}_k)\}$, using (44), with the recursion (12). This recursion starts at a sufficiently negative value of j where we approximate $A_{-,j}$ and $B_{-,j}$ to be 1 and 0, respectively.

In the context of the present discussion, the reflection coefficient $r(w)$, on the unit circle, and the bound states are entirely independent of one another. This possibility is another feature that is unique to our algorithm. In this generality it is difficult to retain control on the duration of the pulse, when there are bound states. In applications to MR, the reflection coefficient extends as a meromorphic function with poles in the unit disk. The data

specifying the bound states is often taken from the singular parts of r at these poles. In this way one regains some control on the duration of the pulse.

4. Practical pulse synthesis

In the previous section we derived recursions for determining the coefficients $\{\gamma_j\}$, which in turn gives the desired hard pulse. What remains is to describe how to obtain a pulse starting from an ideal magnetization profile $\boldsymbol{M}_i(\xi)$ on the real axis, and data specifying bound states. We first describe the data for the right Marchenko equation. The calculation of the data for the left equation is described in the next section.

From Eq. (6), we see that $\boldsymbol{M}_i(\xi)$ defines an ideal reflection coefficient, $r_i(\xi)$. The first step is to approximate $r_i(\xi)$, on a fixed finite interval, by a Fourier series in $w = \mathrm{e}^{2\mathrm{i}\xi\Delta}$. To find a minimum energy pulse, we approximate r_i by a function r with a Fourier series of the form

$$r(w) = \sum_{j=1-\rho}^{M} \hat{r}(n) w^n. \tag{45}$$

Note that $w^{\rho-1} r(w)$ is a polynomial, so $r(w)$ could be found using a Remez-type algorithm. One specifies transition widths, and in-slice and out-of-slice ripples. These parameters, along with the rephasing time, are of course related. In general, once the rephasing time is fixed then, within certain bounds, two of the other three parameters can be specified. These parameter relations are described in detail in [7], see also Section 5. The pulse defined by $r(w)$ alone (without any bound states) has ρ rephasing time steps.

Note that, under the map $\xi \mapsto \mathrm{e}^{2\mathrm{i}\xi\Delta}$, the upper half plane maps to the unit disk. The time spacing, Δ must be chosen so that the range of frequencies of interest lies in an interval of the form $I = [-(2\Delta)^{-1}\pi, (2\Delta)^{-1}\pi]$. The ideal reflection coefficient is assumed to vanish outside this interval. For applications, such as self refocused pulses, different sorts of approximations may be more appropriate. We return to this in Section 4.2.

4.1. The explicit algorithms

In Eqs. (42) and (44) we give expressions for the coefficients $\{\gamma_j\}$ that involve computing Fourier transforms. These formulas can be made much more explicit by introducing the right and left Marchenko kernels. Given $r(w)$, as a Fourier series and pairs $\{(\zeta_1, c_1), \ldots, (\zeta_m, c_m)\}$, describing the bound states, the right Marchenko kernel is defined to be

$$f(n) = \hat{r}(n) - \sum_{k=1}^{m} c_k \zeta_k^{-n} \quad \text{for } n \in \mathbb{Z}. \tag{46}$$

Note that the finite sum is exponentially decreasing as n tends to $-\infty$ and exponentially increasing as n tends to $+\infty$. It is this exponential growth that necessitates the introduction of the left Marchenko equation when there are nontrivial bound states. After determining $a(w)$, $b(w)$, (via Eqs. (18) and (19)), and therefore $s(w)$, and the left norming constants (via Eq. (37)), the left Marchenko kernel is given by

$$g(n) = \hat{s}(n) - \sum_{k=1}^{m} \tilde{c}_k \zeta_k^{-n-1} \quad \text{for } n \in \mathbb{Z}. \tag{47}$$

The role of the bound states in the structure of the Marchenko kernels exactly parallels the situation in the continuum theory. Putting the pieces together, we can write down the explicit algorithms in terms of the left and right Marchenko kernels. We need to select a starting point for each recursion. If we have fixed the rephasing time, so that $f(n) = 0$ for $n \leqslant -\rho$ then we take $N_{\max} = \rho$. Otherwise we check the coefficients $f(n)$, and choose $N_{\max}$ so that

$$\sum_{n=N_{\max}}^{\infty} |f(-n)| \tag{48}$$

is smaller than a fixed tolerance $\epsilon > 0$. Generally speaking $g(n)$ will not vanish for sufficiently negative n. The starting point for the left recursion is therefore selected according to the latter criterion: we choose $N_{\min} < 0$ so that

$$\sum_{n=-\infty}^{N_{\min}-1} |g(n)| < \epsilon. \tag{49}$$

With these choices we start the recursion by setting:

$$\begin{aligned}
&\text{(right)} \quad \begin{cases} K_{+,N_{\max}}(0) = 1, & K_{+,N_{\max}}(n) = 0 \quad \text{for } n > 0, \\ L_{+,N_{\max}}(n) = 0 & \text{for } n \geqslant 0, \end{cases} \\
&\text{(left)} \quad \begin{cases} K_{-,N_{\min}}(0) = 1, & K_{-,N_{\min}}(n) = 0 \quad \text{for } n > 0, \\ L_{-,N_{\min}}(n) = 0 & \text{for } n \geqslant 0. \end{cases}
\end{aligned} \tag{50}$$

Then, with the formulas:

$$\gamma_j = \frac{\sum_{n=0}^{\infty} f(-n-j) K_{+,j+1}(n)}{K_{+,j+1}(0) - \sum_{n=0}^{\infty} f(-n-j) L_{+,j+1}(n)}, \tag{51}$$

$$-\gamma_{j-1}^{*} = \frac{\sum_{n=0}^{\infty} g(-n+j-1) K_{-,j-1}(n)}{K_{-,j-1}(0) - \sum_{n=0}^{\infty} g(-n+j-1) L_{-,j-1}(n)}, \tag{52}$$

$$\alpha_j = (1 + |\gamma_j|^2)^{-1/2},$$

we have the recursions:

$$\begin{aligned}
&\text{(right)} \quad \begin{cases} K_{+,j}(n) = \alpha_j \left[K_{+,j+1}(n) + \gamma_j L_{+,j+1}(n) \right] & \text{for } n \geqslant 0, \\ L_{+,j}(n) = \alpha_j \left[-\gamma_j^{*} K_{+,j+1}(n-1) + L_{+,j+1}(n-1) \right] & \text{for } n \geqslant 1, \\ L_{+,j}(0) = 0. \end{cases} \\
&\text{(left)} \quad \begin{cases} K_{-,j}(n) = \alpha_j \left[K_{-,j-1}(n) - \gamma_{j-1}^{*} L_{+,j-1}(n) \right] & \text{for } n \geqslant 0, \\ L_{-,j}(n) = \alpha_j \left[\gamma_{j-1} K_{-,j-1}(n-1) + L_{-,j-1}(n-1) \right] & \text{for } n \geqslant 1, \\ L_{-,j}(0) = 0. \end{cases}
\end{aligned} \tag{53}$$

These formulas allow for a recursive determination of the coefficients $\{\mu_j\}$ defining the hard pulse with the given scattering data.

A good rule of thumb for switching from the right to left recursion is to switch at an index j_0 for which

$$\sum_{n=j_0+1}^{\infty} |f(-n)| \approx \sum_{n=-\infty}^{j_0-1} |g(n)|. \tag{54}$$

4.2. Bound states with specified rephasing time

In the generality described in Section 4.1, one does not have direct control over either the rephasing time or the duration of the pulse. If there are no bound states, then approximating r_i by a Fourier series of the type given in Eq. (45) leads to a pulse with ρ rephasing steps. If one wishes to use bound states, then they must be selected carefully, to retain control over the rephasing time. In this case, the data describing the bound states is usually derived from the approximation of the reflection coefficient itself. To be able to use the left equation accurately, it is better to describe the approximation to r in a slightly different way.

If one wishes to include bound states, then, instead of using a polynomial to approximate $r_i(\xi)$, we approximate it by a rational function

$$r(w) = \frac{P(w)}{Q(w)}, \tag{55}$$

so that $r(w)w^{\rho-1}$ is analytic, and *nonvanishing* in a neighborhood of 0. To that end, one determines locations, $\{\zeta_1, \ldots, \zeta_m\}$, for the zeros of $Q(w)$ (in addition to the zero at $w = 0$), and looks for a rational function, having poles in that set, which gives an "optimal" approximation to r_i. One can do this iteratively, moving the poles to obtain a better approximation to r_i, subject to a constraint like

$$-\sum_{j=1}^{m} \log|\zeta_j| \leqslant E, \tag{56}$$

so as to not introduce too much additional energy. An example of an algorithm for doing this is given in Section 6.1.

Specifying the locations of the zeros of $Q(w)$, in advance, removes the burden of trying to locate the zeros of $a(w)$, a posteriori. In practice, it is very difficult to determine these zeros accurately enough to use the left equation. In the Appendix we explain how to find a polynomial $D(w)$, so that, $Q(w)/D(w)$ is analytic in the unit disk, positive at $w = 0$ and, for w on the unit circle, we have

$$\left|\frac{P(w)}{D(w)}\right|^2 + \left|\frac{Q(w)}{D(w)}\right|^2 = 1. \tag{57}$$

Hence, $a = Q/D$ and $b = P/D$ are rational functions. In this case, the bound states are given by the zeros $\{\zeta_1, \ldots, \zeta_m\}$ of $Q(w)$ in the set $\{w\colon 0 < |w| < 1\}$. If the pulse is to have ρ rephasing time step, then $Q(w)$ must have a zero of order $\rho - 1$ at zero. With the right norming constants defined to be

$$c_k = \frac{P(\zeta_k)}{Q'(\zeta_k)}, \tag{58}$$

it follows from the assumption that $w^{\rho-1}r(w)$ is analytic in a neighborhood of 0 that $r_j(w) = 0$, for $j \geqslant \rho - 1$. The data for the left Marchenko equations is determined using Eqs. (36) and (37). The left norming constants are

$$\tilde{c}_k = -\frac{\zeta_k D^2(\zeta_k)}{P(\zeta_k)Q'(\zeta_k)}, \tag{59}$$

and

$$s(w) = -\frac{P^*(w)D(w)}{Q(w)D^*(w)}. \tag{60}$$

4.3. Pulse length determination for IST pulses

As noted earlier, for an IST pulse the sequence $\{\mu_j\}$ is, in principle, nonzero as j tends to $-\infty$. In practice, one selects a tolerance to cut the pulse off at a finite j. In this section, we illustrate the effects on the magnetization profile of truncating IST pulses. For this purpose we begin with a minimum energy 90° pulse designed to have a bandwidth of 2 kHz, a transition width of 0.3 kHz and 3 ms of rephasing time. The out of slice ripple is set to 0.01. This pulse was obtained using only the recursion coming from the right Marchenko equation. For a pulse such as that shown in Fig. 1A, the "Connolly wings" are the abrupt jumps in amplitude near the start and finish of the pulse profile. In this example, we see that cutting off the part of the pulse prior to the first Connolly wing leads to a very small in-slice phase error, without any noticeable effect on the selectivity of the pulse. In our experience, this is typical of minimum energy pulses. Pulses with bound states may not have Connolly wings and we do not yet have a good theory for how they should be truncated.

Fig. 1A shows the "reference" pulse, which is sufficiently long to achieve the design specifications. In Figs. 1C and E, we have cut off the indicated amounts from the left-side of the pulse in Fig. 1A. In Figs. 1B, D, and F we show the transverse profiles that result from these pulses. As we see in the next section, a truncated IST pulse still gives better control of the in-slice phase than a comparable SLR pulse.

5. A comparison of SLR and DIST pulse design

We compare the SLR and DIST approaches for designing a minimum energy, 90° pulse in terms of the standard design parameters, in-slice error, out-of-slice error, and transition width. The pass bandwidth is fixed

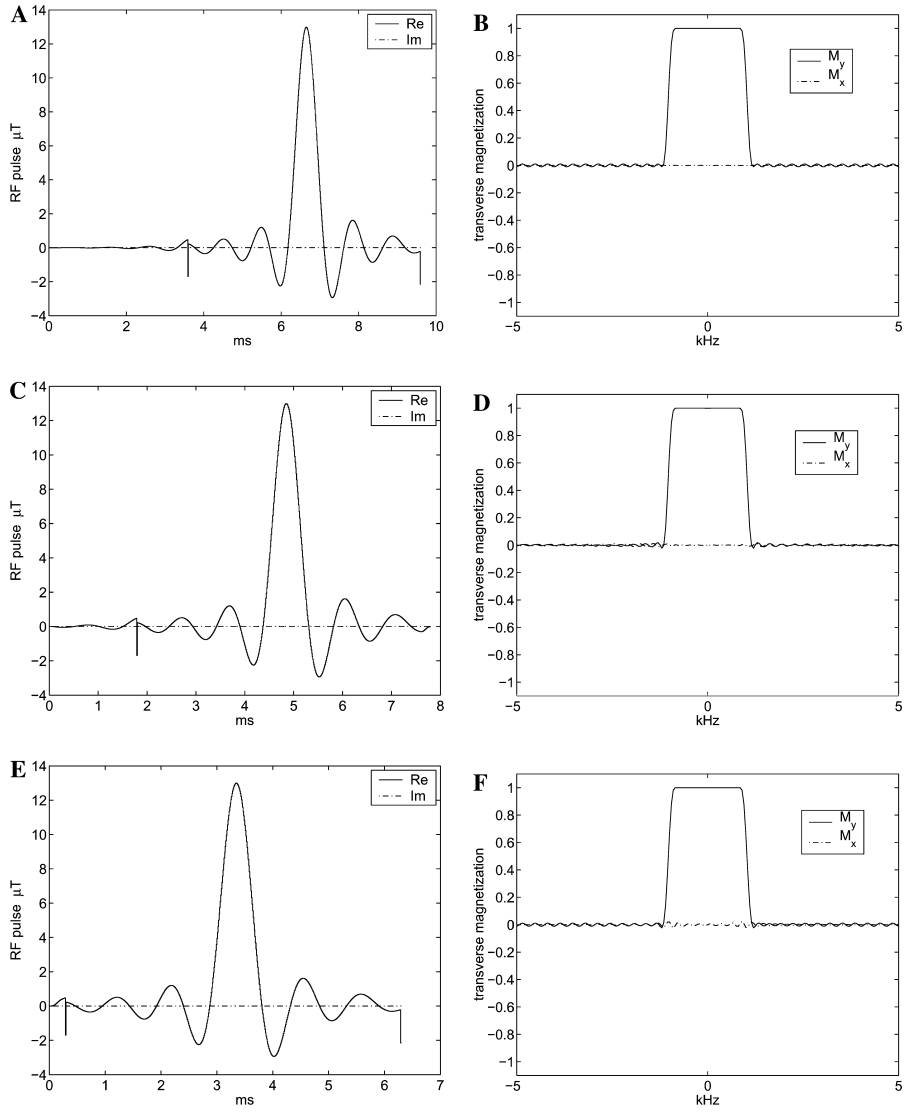

Fig. 1. A 90° DIST pulse with rephasing time = 3.0 ms, transition width = 0.3 kHz, and $\delta_2 = 0.01$. (A) The untruncated pulse, (C) The pulse in (A) truncated by 1.75 ms. (E) The pulse in (A) truncated by 3.57 ms. The corresponding transverse profiles are shown in (B, D, and F).

at 2 kHz in all these examples. The ideal in-slice magnetization profile is

$$M_I(v) = \begin{bmatrix} 0 \\ 1 \\ 0 \end{bmatrix} \quad \text{for } |v| < 1 - \frac{\tau}{2} \tag{61}$$

and the ideal out-of-slice magnetization profile is

$$M_I(v) = \begin{bmatrix} 0 \\ 0 \\ 1 \end{bmatrix} \quad \text{for } |v| > 1 + \frac{\tau}{2}. \tag{62}$$

The number $\tau > 0$ is called the *transition width*. We compare the accuracy of the two approaches using the following parameters:

$$\delta_1 = \text{in-slice error in } M_z \tag{63}$$

$$\delta_2 = \text{out-of-slice error in } |M_x + \mathrm{i}M_y|. \tag{64}$$

Minimum energy SLR pulses are usually designed so that $B(w)$ has "linear" phase. As explained in [4], this implies that $q_\Omega(t)$ is an even function of time. For such a pulse, the rephasing time equals half the duration of the pulse. This is also why SLR pulses of this type produce a phase error in the magnetization profile. Because they do not introduce this phase error, pulses designed using the DIST method are usually *not* time symmetric. The DIST pulses tend to be a little longer than twice the rephasing time.

In Fig. 2, we compare pulses with the same bandwidth, transition width, out-of-slice error, and duration. For each of the two methods, the in-slice error δ_1 is a function of the out-of-slice error δ_2. The DIST pulse has been truncated; the SLR pulse is then designed using

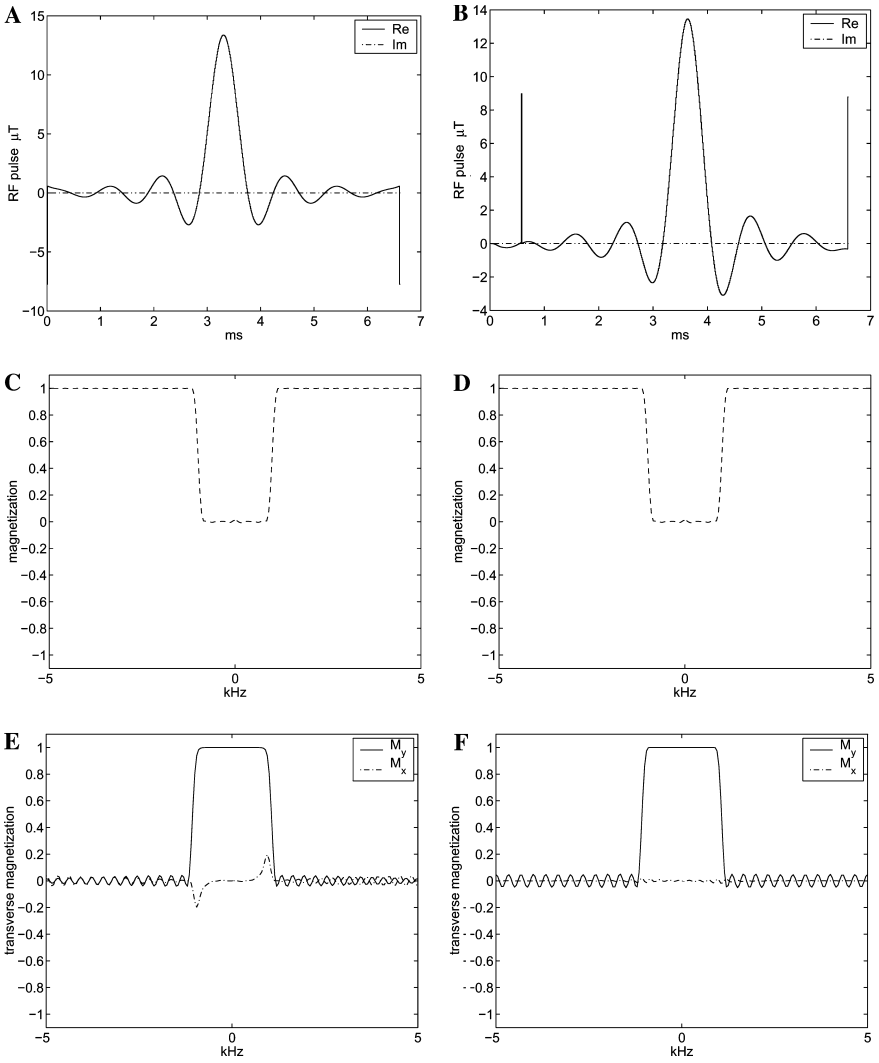

Fig. 2. Comparison of 90°, equiripple SLR and DIST pulses, with equal durations of 6.6 ms, transition width = 0.3 kHz, and $\delta_2 = 0.05$. (A, C, and E) Come from the SLR-pulse and (B, D, and F) from the DIST-pulse; (A and B) show the pulse profiles, (C and D) the longitudinal profiles, and (E and F) the transverse profiles.

the design parameters (out-of-slice error, transition width, etc.) *realized* by the truncated IST pulse. The SLR pulse has been rephased to produce the minimum in-slice phase error. For the SLR pulse, the out-of-slice excitation has both $\boldsymbol{M}_x$ and $\boldsymbol{M}_y$ components, with a fairly complicated phase relation. This makes it somewhat less apparent that this is, in fact, an equiripple pulse.

In Fig. 3 we compare pulses, with identical design parameters, intended to excite two disjoint *in-phase* bands. The SLR pulse is designed using a linear phase B. Figs. 3A and B show the pulses, and Figs. 3C and D show the transverse magnetization profiles. For Fig. 3C, the SLR pulse is rephased so that the two bands are in phase. This leads to a much larger phase error than produced by the DIST pulse. The DIST pulse has slightly more out-of-slice excitation. In Fig. 3E we show the result of rephasing the SLR pulse so that the phase within each band is as close to constant as possible. The phase error within each band is still worse than that produced by the DIST pulse, moreover, the bands are now out of phase with respect to one another. While it may be possible to obtain an SLR pulse that does not produce these phase errors (see the end of this section), the problems encountered here do not arise in the DIST approach.

In the SLR method, one uses the Remez-type algorithm to design a real periodic function

$$B(w) = \sum_{j=1-\rho}^{\rho-1} b_j w^j, \tag{65}$$

such that $B \approx \frac{\sqrt{2}}{2}$ in-slice, and $B \approx 0$ out-of-slice. The polynomial A is then defined by

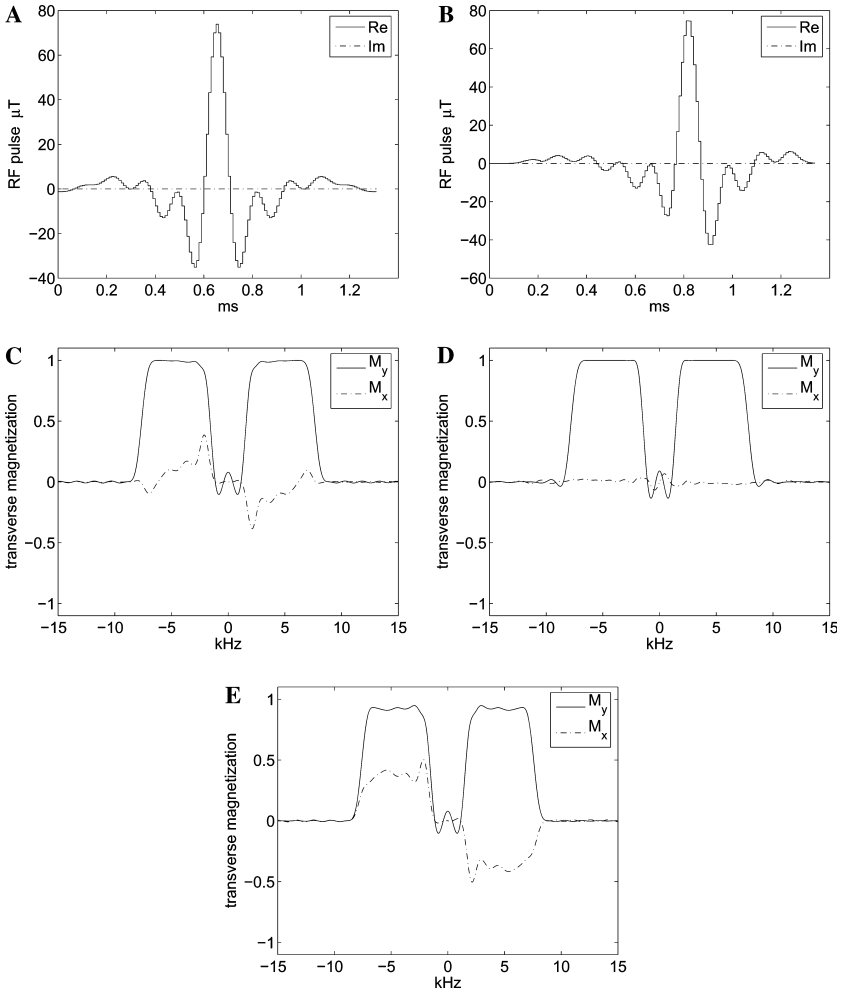

Fig. 3. Comparison of dual band SLR and DIST pulses, with equal design parameters. (A, C, and E) Come from the SLR-pulse, while (B and D) come from the DIST-pulse; (A and B) show the pulse profiles, (C and D) the transverse profiles. The SLR pulse is rephased in (C) so that the two bands are optimally in phase with one another. (E) The result of rephasing the SLR pulse so that the each band has approximately constant phase.

$$A(w) = \exp\left[\tilde{\Pi}_+[\log(1-|b(w)|^2)]\right]. \tag{66}$$

The Remez-type algorithm requires as input the ratio of the following two parameters:

$$\delta_{1,b} = \text{in-slice error in } B, \tag{67}$$

$$\delta_{2,b} = \text{out-of-slice error in } B. \tag{68}$$

One can check that δ_1 and δ_2 are related to these parameters as follows:

$$\delta_1 = 2\sqrt{2}\delta_{1,b} + \delta_{1,b}^2, \tag{69}$$

$$\delta_2 = 2\delta_{2,b}\sqrt{1-\delta_{2,b}^2}. \tag{70}$$

When the rephasing time ρ and the transition width τ are fixed, $\delta_{1,b}$ is a function of $\delta_{2,b}$. An approximate formula for this relationship is given in [9]. Therefore, for the SLR method, δ_1 is a function of δ_2, when ρ and τ are fixed.

The reasoning is similar for the DIST method: one uses Remez-type algorithm to design a real periodic function, $R(w)$ as an approximation to r

$$R(w) = \sum_{j=1-\rho}^{\rho-1} r_j w^j, \tag{71}$$

such that $R \approx 1$ in-slice, and $R \approx 0$ out-of-slice. A Remez-type algorithm requires as input the ratio of the following two parameters:

$$\delta_{1,r} = \text{in-slice error in } R, \tag{72}$$

$$\delta_{2,r} = \text{out-of-slice error in } R. \tag{73}$$

One can check that δ_1 and δ_2 are related to these parameters as follows:

$$\delta_1 = \frac{\delta_{1,r} + \frac{1}{2}\delta_{1,r}^2}{1 - \delta_{1,r} + \frac{1}{2}\delta_{1,r}^2}, \tag{74}$$

$$\delta_2 = \frac{2\delta_{2,r}}{1+\delta_{2,r}^2}. \tag{75}$$

Again, when the rephasing time ρ and the transition width τ are fixed, $\delta_{1,r}$ is a function of $\delta_{2,r}$. Therefore, for the DIST method, δ_1 is a function of δ_2, when ρ and τ are fixed. Note that for a DIST pulse the rephasing time tends to be a little less than half the duration of the pulse.

More generally, the reflection coefficient, r might be a complex valued function. One then uses a complex Remez-type algorithm to find the equiripple approximant, $R(w)$ for r. The phase response of the pulse designed using $R(w)$ as the input to the DIST then accurately reflects the phase of the target profile. In principle, one could also use a complex Remez-type algorithm with the SLR transform as follows: Using Eq. (40) in [4] one determines the scattering coefficient a from r. Next one uses a complex Remez-type algorithm to find the equiripple polynomial approximant $B(w)$ to $b = ra$. Finally, using a Hilbert transform, one determines the polynomial $A(w)$. In practice this turns out to be an unstable procedure. It is hard to get the ratio $B(w)/A(w)$ to be as accurate an approximation to r as $R(w)$. In applications where precise control of the phase of the magnetization profile is important, e.g., half pulse design, the DIST provides an alternative to SLR. The computational requirements of the two algorithms are essentially identical. The price one pays for the phase control provided by the DIST pulse is usually a slightly longer duration pulse.

6. Further examples

This sections contains several more examples illustrating different features of the DIST approach. In Section 6.1, we compare the effect of B_1 amplitude errors on the magnetization profiles produced by several self refocused pulses. In Section 6.2, we give pulses with arbitrarily specified bound states. To the best of our knowledge, this is something that can only be done with the DIST.

6.1. Self-refocused pulses

In some applications it is desirable to use a self-refocused pulse, or a pulse with no rephasing time. It is important to understand the relationships between pulse energy, pulse duration, and the accuracy of the approximation. For example, the more poles we allow $r(w)$ to have, the better the approximation can be. However, according to Eq. (26), each added pole costs energy. In this section, we describe how to practically design relatively low-energy, self-refocused pulses. Thus far, no one has presented a technique for finding pulses of this sort using the SLR approach. They could also be computed using the rational function algorithm described in [2,11].

Let r_i be the ideal reflection coefficient, as a function of the offset frequency v. For example, for a selective 90° pulse, we might have

$$r_i(v) = \begin{cases} 1 & \text{if } |v| < 1, \\ 0 & \text{if } |v| > 1. \end{cases} \tag{76}$$

The goal is to approximate r_i, in a neighborhood of $v = 0$, by a function r of $w = e^{iv\Delta}$, which is meromorphic in the unit disk and analytic at the origin. In this case, we design $r(w)$ as a real valued rational function of w, with simple poles. It is awkward to do this directly, since r_i is a function of v. As a practical alternative, we first approximate $r_i(v)$ by a rational function $\tilde{r}(v)$ of the form

$$\tilde{r}(v) = \sum_{j=0}^{m} \left[\frac{C_j}{v-\eta_j} + \frac{C_j^*}{v-\eta_j^*} \right] \tag{77}$$

for $\eta_1, \ldots, \eta_m$ in $\mathbb{H}$, the upper half complex plane. We then define

$$r(w) = \sum_{j=0}^{m} \left[\frac{iC_j\Delta}{1-e^{i\eta_j\Delta}w^{-1}} - \frac{iC_j\Delta}{2} + \frac{-iC_j^*\Delta}{1-e^{-i\eta_j^*\Delta}w} - \frac{-iC_j^*\Delta}{2} \right]. \tag{78}$$

Notice that, for v in a fixed interval $r(e^{iv\Delta})$, can be made arbitrarily close to $\tilde{r}(v)$ by taking Δ small enough. The contribution of the bound states to the energy of the designed pulse is then approximately $4\sum_{k=1}^{m} \Im\eta_k$. With this choice of bound state data, the right Marchenko kernel, $f(n)$ vanishes for $n > 0$.

There are many possible techniques for choosing the rational function $\tilde{r}(v)$. The method we use to compute the examples shown in Fig. 4 is to first fix m, the number of the poles, and then constrain the locations of the individual poles to lie in certain subsets of the upper half plane. A Newton type algorithm is then used to determine the precise locations of the poles and the norming constants so that the L^2 norm of the error $|\tilde{r} - \tilde{r}_i|$ is made as small as possible. As is often the case when using rational approximations (instead of polynomials), this optimization problem has many local minima, producing dramatically different pulses. All the pulses produce essentially the same magnetization profile. In general, poles close to the x-axis add relatively little energy, but tend to result in longer pulses, whereas poles with large imaginary parts tend to yield shorter, high energy pulses. The pulses designed here have much less additional energy, due to bound states, than the examples given in [11].

The poles (that is the $\{\eta_j\}$ in Eq. (77)) for Fig. 4A are located at $\{0.35i \pm 0.9,\ 0.4i \pm 0.15\}$, for Fig. 4B at $\{0.4i \pm 0.4,\ 0.3i \pm 0.85\}$. These are shown in Fig. 5. Figs. 4C and D show the transverse profiles produced

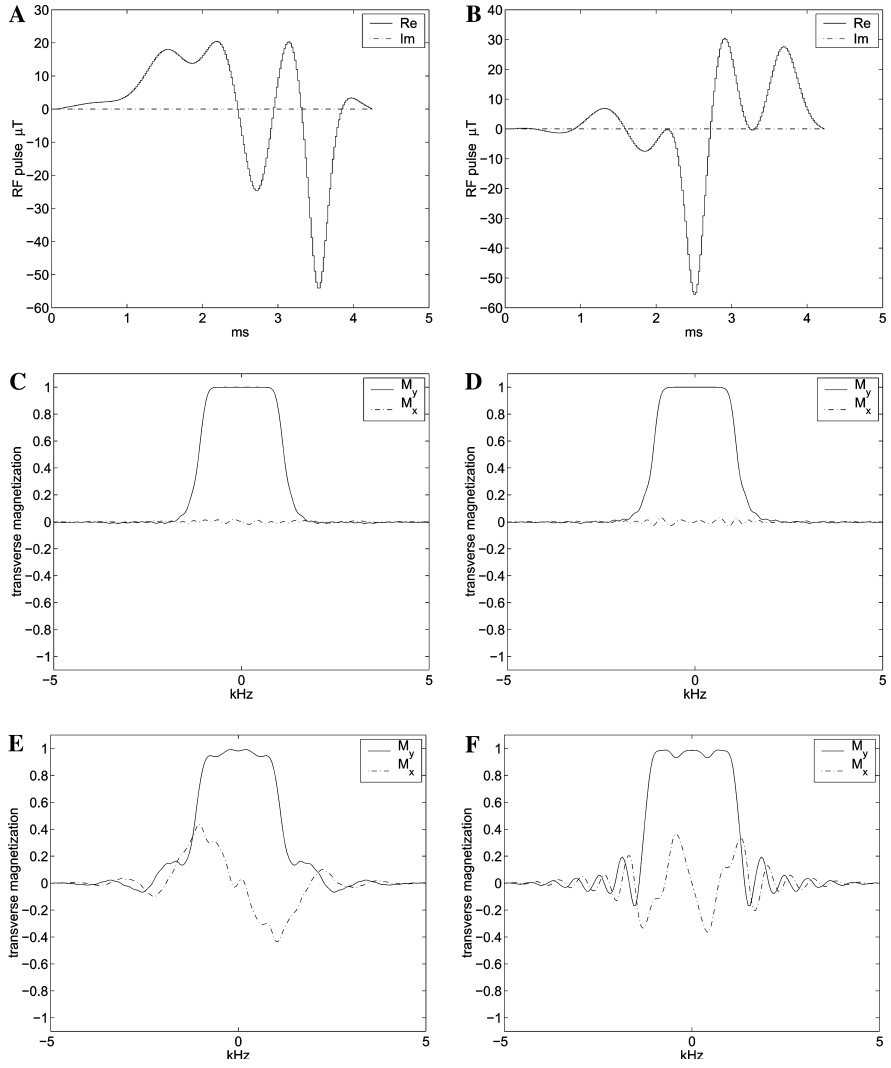

Fig. 4. Two self refocused 90° pulses. The pulses shown in (A and B) were designed by using different rational approximations, $r(w)$ for the desired reflection coefficient. The poles of $r(w)$ in the unit disk were then used to define the bound states. As expected this produces a pulse which requires no rephasing time. Both pulses have a duration between 4 and 5 ms. (C and D) The transverse magnetization profiles produced by these pulses. (E and F) The transverse profiles obtained if the pulses are scaled by 0.9. The locations of the poles are shown in Fig. 5.

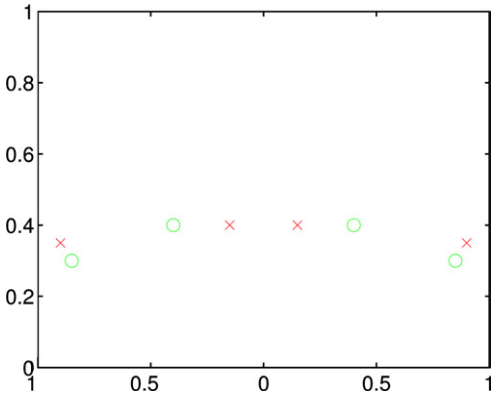

Fig. 5. The locations of the poles for the pulses shown in Figs. 4A and B, with (A), ×; (B), ○.

by these pulses and Figs. 4E and F the transverse profiles when the amplitudes of the pulses are scaled by 0.9. These pulses are considerably more sensitive to amplitude errors than a comparable minimum energy pulse. The total energies for these pulses are 2.0374 kHz^2ms for (a) and 1.9096 kHz^2ms for (b). A comparable minimum energy pulse has total energy 0.1347 kHz^2ms.

The B_1-amplitude error causes the self refocused pulses to become less selective and decreases the in-slice phase control. The effects on the two pulses are quite different, with the higher energy pulse faring worse. Self refocused pulses are less sensitive to a small T_2 than a minimum energy pulse would be. In the interest of saving space we do not show an example of this effect. While we do not yet know how to design "optimal" self refocused pulses, the DIST algorithm makes it possible to empirically study this problem. The problem of how best to use rational functions to approximate a function, for the purposes of RF-pulse design, is an interesting new direction for research.

6.2. Arbitrary bound states

Our last group of examples demonstrates that arbitrary bound states can be incorporated using the DIST approach. Fig. 6 shows two pulses, and the transverse magnetization profiles they generate. Each pulse is generated using a single reflection coefficient, along with data specifying bound states. The bound states in these examples are specified in terms of the continuum inverse scattering data, i.e., the location of the poles and norming constants, $\{(\eta_j, C_j)\}$, as in Eq. (77). The pulses are evidently quite different from one another, but nonetheless, produce the same transverse magnetization profile. While pulses with bound states unconnected to the reflection coefficient may not have immediate applications in MR, the design of such pulses is a *unique* capability of the DIST approach that we wanted to demonstrate.

7. Conclusion

In this paper, we have derived a practical algorithm which implements the approach to pulse design via the inverse scattering transform described in [4]. The algorithm uses the idea of the hard pulse approximation, which is also employed in the layer stripping and SLR approaches. There are two principal differences: (1) We work, throughout the design process, with the full magnetization profile. In most implementations of SLR only the flip angle profile is used, and direct control on the phase of the transverse magnetization is difficult to attain. (2) We use a different recursive algorithm to recover the hard pulse from the scattering data. This algorithm, which is a discrete version of the Marchenko equation formalism from inverse scattering theory, allows for the inclusion of arbitrary bound states. In computer trials we have found our recursion to be as fast as

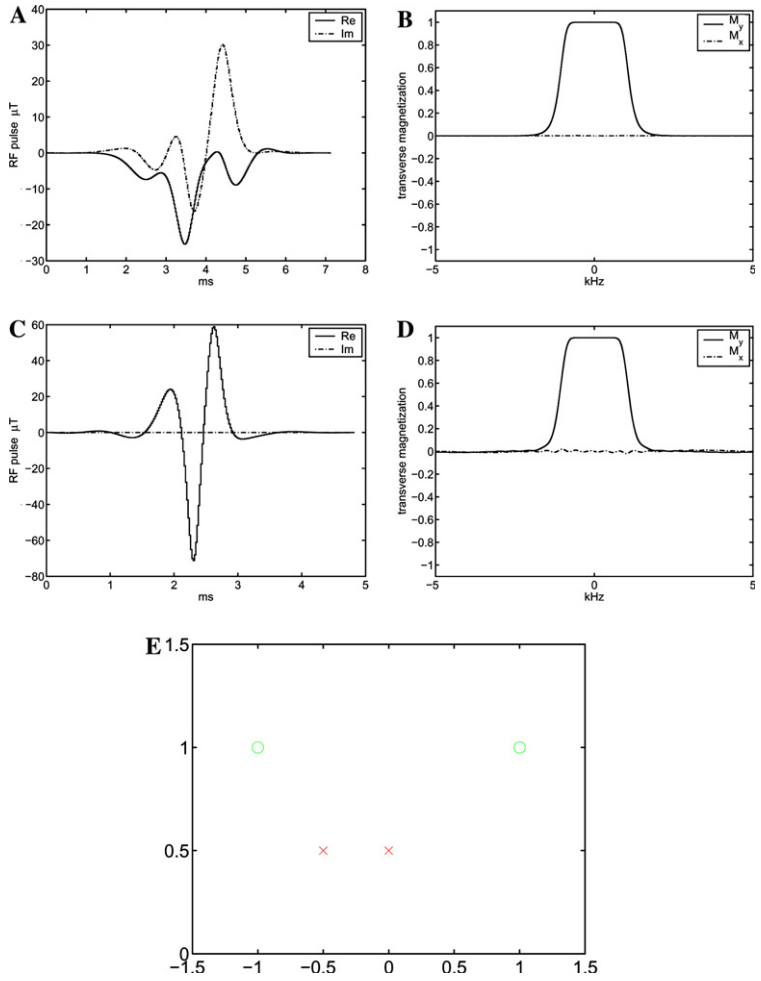

Fig. 6. Two 90° pulses illustrating the possibility of adding arbitrary bound states. These pulses were obtained by augmenting the magnetization profile data with the indicated bound states. To the right of the pulse is the transverse magnetization profile it generates (B and D), respectively. (A) Bound states located at $0.5i - 0.5$ and $0.5i$ with norming constants: 1 and 1, (C) bound states located at $i - 1$, $i + 1$, with norming constants i and i. These are shown in (E) with (A), × and (C), ○.

the standard SLR approach. By using both the left and right Marchenko equations, we are able to control the instabilities, described in [4], which arise in the solution of the pulse synthesis problem when bound states are present.

We call our approach the discrete inverse scattering transform or DIST. Using the DIST, we recover the full range of the solutions to the pulse design problem, present in the continuum model. In particular, for a fixed magnetization profile, there is an infinite dimensional space of DIST pulses that produce the desired profile. The DIST is the first efficient and stable ''general purpose'' approach to pulse design. Using it one can obtain all pulses one could obtain using earlier approaches, in addition one is now free to explore the effects of adding bound states.

Earlier approaches to pulse design made extensive usage of an analogy between pulse design and FIR filter design. While there are points of contact between the two subjects, and the approximation techniques developed for filter design are an essential component of pulse design, the two subjects are essentially different. The pulse design is highly nonlinear, with an infinite dimensional space of solutions to each and every problem. This nonuniqueness is entirely lost in the filtering analogy. Beyond any technical advances, we feel that the most important lesson we have learned is that the inverse scattering formalism provides the correct conceptual framework and language for pulse design. The bound states present a great opportunity for new solutions to old problems as well as entirely new avenues of research. To make significant progress in this field, we will need to come to grips with this fundamental feature of the pulse design problem. The DIST provides the practical tools needed to begin a systematic study of these questions.

Acknowledgment

We thank the referees for their careful assessments of our paper and their many useful suggestions.

Appendix A. Rational reflection coefficients

Let $r(w)$ be a rational function and let $a(w)$ and $b(w)$ be functions, with $a(w)$ analytic in the unit disk, and nonvanishing at 0, such that, on the unit circle, we have

$$|a(w)|^2 + |b(w)|^2 = 1 \quad \text{and } r(w) = \frac{b(w)}{a(w)}. \tag{A.1}$$

In this Appendix we show that $a(w)$ and $b(w)$ are rational functions.

Proof. Since r is a rational function we can write

$$r(w) = \frac{P(w)}{Q(w)}, \tag{A.2}$$

where $P(w)$ and $Q(w)$ are polynomials with no common zeros. By the lemma below, we can express

$$P^*P + Q^*Q = \tilde{D}^*\tilde{D}, \tag{A.3}$$

where $\tilde{D}$ is a polynomial that does not vanish in the unit disk. Let ρ denote the order of vanishing of $Q(w)$ at $w = 0$ and set $D(w) = w^\rho \tilde{D}(W)$. We let

$$A(w) = \frac{Q(w)}{D(w)}, \quad B(w) = \frac{P(w)}{D(w)}, \tag{A.4}$$

so that $r = \frac{B}{A}$ and $|A|^2 + |B|^2 = 1$. Furthermore, $A(w)$ is analytic in the unit disk, with $A(0) \neq 0$. It follows that $a(w) = e^{i\varphi}A(w)$ for a real constant φ. This phase is determined so that $a(0)$ is a positive real number. □

Lemma 1. *If $P(w), Q(w)$ are polynomials without common zeros, then there exists another polynomial $\tilde{D}(w)$, which does not vanish in the unit disk, such that, on the unit circle, we have*

$$\tilde{D}^*\tilde{D} = P^*P + Q^*Q. \tag{A.5}$$

Proof. Let $F(w) = P^*P + Q^*Q$. It has the form

$$F(w) = \sum_{j=-n}^{n} c_j w^j, \tag{A.6}$$

which factors as

$$F(w) = \lambda \prod_{k=1}^{m}(w - \alpha_k)\prod_{k=1}^{m}(w^{-1} - \alpha_k^*). \tag{A.7}$$

Here the $\{\alpha_k\}$ lie inside the unit disk. The function has this form because it is real on the unit circle. In this case λ is a positive real number, and we set

$$\tilde{D}(w) = \sqrt{\lambda}\prod_{k=1}^{m_1}(1 - w\alpha_k^*). \qquad \square \tag{A.8}$$

We finish this Appendix by showing how, in practice, $\tilde{D}(w)$ is determined. The function $\log F(w)$ extends to define an analytic function in a neighborhood of the unit circle, with

$$\log F(w) = \sum_{n=-\infty}^{\infty} b_n w^n. \tag{A.9}$$

One can show that

$$\Pi_-(\partial_w \log F)(w) = \sum_{k=1}^{m}\frac{1}{w - \alpha_k} - \frac{m}{w}. \tag{A.10}$$

Integrating this expression along the unit circle, from 1 to w, we obtain that

$$\prod_{k=1}^{m}(w-\alpha_k) = w^m\left[\exp\left(\sum_{n=-\infty}^{-1} b_n w^n\right)\right]_{-m}. \tag{A.11}$$

Here the notation $[\cdot]_{-m}$ is defined by

$$\left[\sum_{n=-\infty}^{-1} a_n w^n\right]_{-m} = \sum_{-m}^{-1} a_n w^n. \tag{A.12}$$

The polynomial $\tilde{D}(w)$ is readily determined once $\prod_{k=1}^{m}(w-\alpha_k)$ is known. Observe that all that is required is the computation of the Fourier coefficients $\{b_{-1},\ldots,b_{-m}\}$, which can be done quickly, with very high precision, using the FFT.

References

[1] M. Buonocore, The analytic theory, optimization, and performance of transparent pulses, Magn. Reson. Med. 24 (1992) 314–324.
[2] M. Buonocore, RF pulse design using the inverse scattering transform, Magn. Reson. Med. 29 (1993) 470–477.
[3] J.W. Carlson, Exact solutions for selective excitation pulses, J. Mag. Reson. 94 (1991) 376–386.
[4] C.L. Epstein, Minimum power pulse synthesis via the inverse scattering transform, J. Magn. Reson. 167 (2004) 185–210.
[5] L. Faddeev, L. Takhtajan, Hamiltonian Methods in the Theory of Solitons, Springer, Berlin, Heidelberg, New York, 1987.
[6] J. Magland, The selective excitation transform and NMR pulse design. PhD. Thesis, University of Pennsylvania, 2004.
[7] J. Pauly, P. Le Roux, D. Nishimura, A. Macovski, Parameter relations for the Shinnar–Le Roux selective excitation pulse design algorithm, IEEE Trans. Med. Imaging 10 (1991) 53–65.
[8] S. Pickup, X. Ding, Pulses with fixed magnitude and variable phase response profiles, Magn. Reson. Med. 33 (1995) 648–655.
[9] L. Rabiner, B. Gold, Theory and Application of Digital Signal Processing, Prentice Hall, Englewood Cliffs, NJ, 1975.
[10] T. Rivlin, An Introduction to the Approximation of Functions, Dover Publications, New York, 1969.
[11] D.E. Rourke, P.G. Morris, The inverse scattering transform and its use in the exact inversion of the Bloch equation for noninteracting spins, J. Magn. Reson. 99 (1992) 118–138.
[12] D.E. Rourke, J.K. Saunders, A simple relationship between total RF pulse energy and magnetization response—The nonlinear generalization of Parseval's relation, J. Magn. Reson. Ser. A 115 (1995) 189–196.
[13] M. Shinnar, S. Eleff, H. Subramanian, J. Leigh, The synthesis of pulse sequences yielding arbitrary magnetization vectors, Magn. Reson. Med. 12 (1989) 74–88.
[14] M. Shinnar, J. Leigh, Inversion of the Bloch equation, J. Chem. Phys. 98 (1993) 6121–6128.